



The potential of polarization measurements from space at mm and sub-mm wavelengths for determining cirrus cloud parameters

J. Miao, K.-P. Johnsen, S. Buehler, A. Kokhanovsky

► To cite this version:

J. Miao, K.-P. Johnsen, S. Buehler, A. Kokhanovsky. The potential of polarization measurements from space at mm and sub-mm wavelengths for determining cirrus cloud parameters. *Atmospheric Chemistry and Physics*, 2003, 3 (1), pp.39-48. hal-00295221

HAL Id: hal-00295221

<https://hal.science/hal-00295221>

Submitted on 28 Jan 2003

HAL is a multi-disciplinary open access archive for the deposit and dissemination of scientific research documents, whether they are published or not. The documents may come from teaching and research institutions in France or abroad, or from public or private research centers.

L'archive ouverte pluridisciplinaire **HAL**, est destinée au dépôt et à la diffusion de documents scientifiques de niveau recherche, publiés ou non, émanant des établissements d'enseignement et de recherche français ou étrangers, des laboratoires publics ou privés.

The potential of polarization measurements from space at mm and sub-mm wavelengths for determining cirrus cloud parameters

J. Miao¹, K.-P. Johnsen², S. Buehler¹, and A. Kokhanovsky¹

¹Institute of Environmental Physics, University of Bremen, Germany

²GKSS Research Center Geesthacht GmbH, Geesthacht, Germany

Received: 30 August 2002 – Published in Atmos. Chem. Phys. Discuss.: 19 September 2002

Revised: 15 November 2002 – Accepted: 20 December 2002 – Published: 28 January 2003

Abstract. The millimeter and sub-millimeter waves have been attracting a lot of attention recently in the cloud remote sensing community. This is largely because of their potential use in measuring cirrus cloud parameters with airborne or space-borne radiometers. In this study, we examine the possibility of using polarization measurements in this frequency range to get information on the microphysical properties of cirrus clouds. By using a simple radiative transfer model, we calculated the brightness temperature differences at the vertical and horizontal polarization channels for the following seven frequencies: 90, 157, 220, 340, 463, 683, and 874 GHz. The ice crystals in cirrus clouds are modeled with nearly spherical particles, circular cylinder, and circular plate, as well as with mixtures of these types. We found that the polarization difference signal shows a unique “resonance” feature with the change of ice particle characteristic size: it has a strong response only in a certain range of ice particle size, beyond that range it approaches zero. The size range where this resonance happens depends to a large extent on particle shape and aspect ratio, but to a much less extent on particle orientation. This resonance feature appears even when ice clouds are composed of a mixture of ice crystals in different shapes, although the magnitude and the position of the resonance peak may change, depending on how the mixture is made. Oriented particles generally show larger polarization difference than randomly oriented ones, and plates have larger polarization difference than cylinders. However, the state of particle orientation has a significantly stronger effect on the polarization difference than the particle shape (cylinder or plate). This makes it difficult to distinguish particle shapes using millimeter and sub-millimeter radiometric measurements, if there is no information available on particle orientations. However, if the state of particle shape mix-

ture can be predetermined by other approaches, polarization measurements can help to determine ice particle characteristic size and orientation. This information, in turn, will benefit our retrieval of the ice water path of cirrus clouds.

1 Introduction

In the last two decades many studies have been carried out for the remote sensing of cirrus clouds from ground, airplane, and satellites (Lynch et al., 2002). Both active and passive approaches have been tested. Most of them are exploiting the advantages of the visible, infrared, and microwave range of the electromagnetic spectrum. Recently, the millimeter (mm) and sub-millimeter (sub-mm) wave range, which covers frequencies from about 150 to about 1000 GHz with corresponding wavelength ranging from 2.0 to 0.3 mm, has been explored. Both theoretical simulations and experimental studies have been conducted. The results show that this spectral range could be very promising in measuring cloud parameters such as the ice water path (IWP) and the ice particle characteristic size (Evans et al., 1998; Wang et al., 2001).

The mm and sub-mm range shows some important advantages compared with the other commonly used spectral ranges. First of all, the wavelengths in this range are comparable with or larger than the sizes of most ice particles. Secondly, the imaginary part of the refractive index of pristine ice in the mm and sub-mm spectrum is much smaller than the real part of the refractive index. These two factors combined cause the interaction between ice particles and the atmospheric radiation to be dominated by the scattering effect, which is almost independent of the ambient temperature of the cloud and mainly related to the volume (or mass) of the ice particles. Furthermore, because of the strong absorption of atmospheric water vapor, ground surface is almost unde-

Correspondence to: J. Miao (jmiao@uni-bremen.de)

tectable for a space-borne mm and sub-mm radiometer. Finally, since cirrus clouds are mostly thin, the brightness temperature depressions induced by cloud ice particle scattering are, in most cases, proportional to the cloud IWP, at the mm and sub-mm frequencies (Liu and Curry, 2000). This will significantly simplify the retrieval of cloud parameters from radiometric measurements.

However, until now most studies are concerned with the information content of radiometric intensity signals (Evans et al., 1998; Wang et al., 2001). Frankly speaking, there is a general lack of studies on the potential of polarization measurements in the mm and sub-mm wave band. In this paper, we will treat this topic in some detail. As mentioned earlier, the ground surface is mostly undetectable for a space-borne mm and sub-mm radiometer, except for the two lowest frequencies at 90 and 157 GHz considered in this paper, at which the ground surface contribution can be significant in dry atmospheric situations. In our later simulations, we ignore the surface contribution at these two frequencies and at other frequencies as well. Under this condition, the polarization signal is exclusively induced by the scattering of frozen hydrometeors, i.e. ice crystals to the unpolarized atmospheric radiations. By using a simple physical model, we demonstrate in Sect. 2 the advantages of polarization measurements. In Sect. 3 we apply this model to cirrus clouds in order to examine factors which influence the polarization signature measured by a space-borne mm and sub-mm radiometer. These factors include particle shape, particle orientation, and particle size. And finally in Sect. 4, we present some discussions and conclude the paper.

2 The physical model

The polarization signature is described by the brightness temperature difference measured by a radiometer at two orthogonally polarized channels, i.e. the vertical and horizontal channels. Highly accurate polarization difference measurements at the microwave band can be achieved with today's technology (Hollinger et al., 1990). The usage of this signature has been shown to be very effective, e.g. in determining surface features as sea ice concentration (Kern and Heygster, 2001) or atmospheric parameters such as rain rate over land (Spencer et al., 1989) and cloud liquid water over sea ice (Miao et al., 2000). To analyze the information content of the polarization signature of cirrus clouds, we use the simple physical model shown in Fig. 1.

In this simple model, the atmosphere is assumed to be in a plane-parallel structure containing only one single layer of ice cloud. The atmosphere has three layers, which are assumed to be homogeneous and isothermal. Only the middle layer contains ice particles. The brightness temperature observed by a space-borne radiometer at the polarization state β is denoted by $T_{b\beta}$ and β can be v or h , respectively for vertical or horizontal polarization. $T_{b\beta}$ can be expressed explicitly

with the physical parameters given for each layer. The reflection and refraction effects at layer boundaries are neglected. Within the cloud layer only single scattering effect is taken into account for the interaction between ice particles and atmospheric radiation. Under these conditions, $T_{b\beta}$ consists of the following four parts: the first part, denoted by $T_{b\beta,1}$, is the emission from gases in the uppermost layer. The second part, $T_{b\beta,2}$, is the emission from the layer containing a cloud, which is attenuated by gaseous absorption in the uppermost layer. The third part, $T_{b\beta,3}$, represents the radiation coming from the lowermost layer, which is attenuated by the overlying two layers through both absorption and scattering. And finally the fourth part, $T_{b\beta,4}$, describes the contribution due to ice particle scattering in the cloud layer. This part is also attenuated by the upper layer absorptions. Summing up all these parts gives

$$T_{b\beta} = T_{b\beta,1} + T_{b\beta,2} + T_{b\beta,3} + T_{b\beta,4} \quad (1)$$

The terms on the right-hand side of Eq. (1) can be explicitly expressed as

$$T_{b\beta,1} = T_1(1 - e^{-\tau_{a1} \sec \theta}), \quad (2)$$

$$T_{b\beta,2} = T_2(1 - e^{-\tau_{a2} \sec \theta})e^{-\tau_{a1} \sec \theta}, \quad (3)$$

$$T_{b\beta,3} = T_3(1 - e^{-\tau_{a3} \sec \theta})e^{-(\tau_{a1} + \tau_{a2} + \tau_{s2,\beta}) \sec \theta}, \quad (4)$$

and

$$T_{b\beta,4} = T_{s\beta}e^{-\tau_{a1} \sec \theta}. \quad (5)$$

Here τ_{ai} ($i \in 1, 2, 3$) is the partial opacity of layer i due to atmospheric absorptions. Theoretically, τ_{a2} includes the effect of cloud ice particle absorptions and consequently it depends also on the polarization state. However, since ice particles absorb little mm and sub-mm wave energy, we hereby neglect their contribution in τ_{a2} . The attenuation caused by ice particle scattering is represented by $\tau_{s2,\beta}$, which depends on the polarization state β . The physical temperature of each layer is denoted by T_i with $i \in 1, 2, 3$. Additionally, $T_{s\beta}$ in Eq. (5) represents the scattering contribution of ice particle scattering, which was made by radiations coming from other directions and scattered toward the radiometer observing direction. This term is directly related to ice particle microphysical properties as particle number, size, shape, and orientation.

Since the first two parts of $T_{b\beta}$, i.e. terms $T_{b\beta,1}$ and $T_{b\beta,2}$, do not depend on the polarization state, these two terms can be canceled by taking differences of the brightness temperatures measured at two orthogonally polarized channels,

$$Q = T_{bv} - T_{bh}. \quad (6)$$

In this way, the polarization difference Q will not depend on atmospheric emissions from the cloud and from the uppermost layer, although the uppermost layer still have influences on Q through the absorption attenuation. This is because of

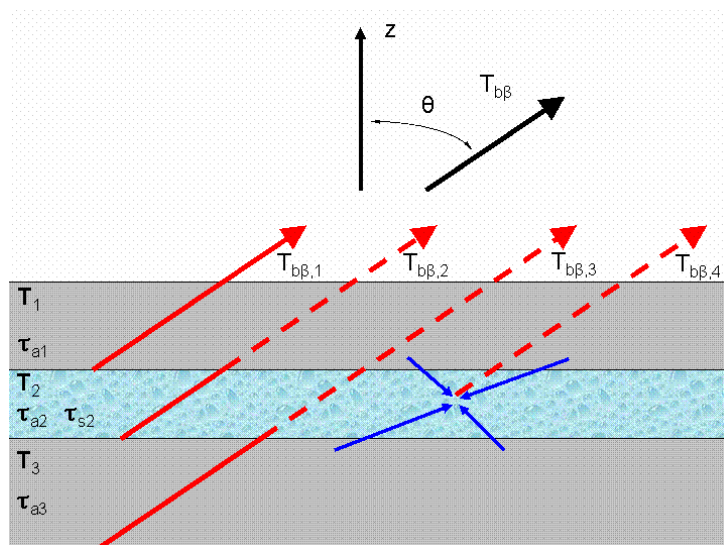


Fig. 1. The geometry of the problem.

the effect of term $e^{-\tau_{a1} \sec \theta}$, which is contained in terms $T_{b\beta,3}$ and $T_{b\beta,4}$.

By defining T_{bL} as

$$T_{bL} = T_3(1 - e^{-\tau_{a3} \sec \theta}), \quad (7)$$

Q can be explicitly written as

$$Q = T_{bL} e^{-(\tau_{a1} + \tau_{a2}) \sec \theta} (e^{-\tau_{s2,v} \sec \theta} - e^{-\tau_{s2,h} \sec \theta}) + (T_{sv} - T_{sh}) e^{-\tau_{a1} \sec \theta}. \quad (8)$$

Note that T_{bL} approaches to the layer air temperature T_3 as the layer opacity τ_{a3} approaches to infinity. The right-hand side of the above equation shows that Q consists of two terms, which describe the contributions from two different sources. The first term represents the direct contribution of the radiation coming from the lowermost layer and traveling through the cloud and the uppermost layer up to the space-borne radiometer. Since the radiation from the lowermost layer is unpolarized (note, the ground surface polarization signal is ignored), the polarization difference is exclusively induced by the different scattering efficiencies of ice particles at the two different polarization states. The second term, in contrast, expresses the contributions of ice particle scattering of the radiation from all directions. The first term will be zero if ice particles are spherical or randomly oriented, because, in this case, ice particle scattering efficiencies are same at the two orthogonal polarization states, i.e. $\tau_{s2,v}$ is equal to $\tau_{s2,h}$. In general, however, the second term is nonzero.

Suppose that we have two different frequencies, f_1 and f_2 , at which the opacities due to atmospheric absorption are same, i.e. $\tau_{ai}(f_1)$ is equal to $\tau_{ai}(f_2)$, for all three layers ($i \in 1, 2, 3$), then the ratio of the two polarization differences $\frac{Q(f_1)}{Q(f_2)}$ will be free of the screening effect (due to both emission and attenuation) of the upper layer. By referring

to Eq. (8), we can understand that this is because the two terms on the righthand side of Eq. (8) contain a common factor $e^{-\tau_{a1} \sec \theta}$. Furthermore, since Q is proportional to T_{bL} , which represents the intensity of radiation coming from the lowermost layer, the ratio $\frac{Q(f_1)}{Q(f_2)}$ is, to some extent, also independent of the atmospheric conditions below the cloud. This will simplify our consequent cloud parameter retrievals. Based on this idea, a recently proposed concept of a space-borne mm and sub-mm radiometer, which is dedicated to cirrus cloud measurements, has included some well-matched frequencies (for details see Miao et al. (2002)).

When the cloud is optically thin, we expect that the polarization difference Q will increase linearly with the increase of cloud optical thickness (ice particle size and/or cloud IWP). If the cloud optical thickness increases continually, Q will reach its saturation due to multiple scattering at a certain amount of cloud optical thickness. How large this amount is depends on the observing frequency. Therefore, simultaneous measurements at two or more frequencies will enable us to cover a large range of cloud particle sizes and optical depths. On the other hand, for thin cirrus clouds where the polarization difference Q has a linear relationship with the cloud IWP, the evaluation of the ratio of polarization differences, $\frac{Q(f_1)}{Q(f_2)}$, can help us, at least to some extent, to get rid of the influence of IWP from the measurements and in such a way to further isolate the information of ice particle microphysical properties. This microphysical property information, when it is available, will help us in the retrieval of cloud IWP.

3 The information content of polarization measurements

3.1 The radiative transfer model

From the physical analysis in the preceding section, we know that the uppermost layer plays a minor role in the polarization signature. Therefore we neglect the effect of the uppermost layer in the following discussions. By further assuming the cloud layer to be thin and omitting the absorption in this layer, we get a simpler form of Eq. (8)

$$Q = Q_s + T_{bL}(e^{-\tau_{s2,v} \sec \theta} - e^{-\tau_{s2,h} \sec \theta}), \quad (9)$$

where $Q_s = T_{sv} - T_{sh}$. From Mishchenko et al. (2000), we get Q_s in the single scattering approximation,

$$Q_s(\mathbf{n}) = N_0 \int_{4\pi} \langle Z_{21}(\mathbf{n}, \mathbf{n}') \rangle I_{in}(\mathbf{n}') d\Omega'. \quad (10)$$

Here, \mathbf{n} and \mathbf{n}' denote the directions of the satellite observation and the incident radiation, respectively. $\langle Z_{21}(\mathbf{n}, \mathbf{n}') \rangle$ is the element (2,1) of the ice particle scattering matrix $\langle \mathbf{Z}(\mathbf{n}, \mathbf{n}') \rangle$, which is ensemble averaged according to ice particle size, shape, and orientation distributions. N_0 is the number density of ice particles in the cloud times the cloud geometrical thickness and it is in a dimension of $1/\text{m}^2$. $I_{in}(\mathbf{n}')$ represents the intensity (in Kelvins) of radiation incident on the particle from a direction \mathbf{n}' .

To make the simulation more close to reality, we used the temperature and humidity profiles (with a surface relative humidity of 80%) of the standard US atmosphere (1976) (Ulaby et al., 1981), instead of the isothermal and homogeneous atmosphere assumed in the physical model presented in the preceding section. The ground surface temperature is set to be equal to the surface air temperature and the surface emissivity is assumed to be 1. There is no polarization difference signal from the ground surface assumed. The exact value of the surface emissivity is relatively arbitrary, since the ground surface is undetectable for most frequencies considered in this study. The thin cirrus cloud layer is placed at the altitude of 10 km. The satellite observation angle θ is fixed at 54° , which is mostly selected by low orbit satellites. T_{bL} and $I_{in}(\mathbf{n}')$ are calculated using the radiative transfer model described by Gasiewski (1993). Since the atmosphere is taken to be plane-parallel, the intensity of the incident radiation, $I_{in}(\mathbf{n}')$, depends only on the incidence angle, which is the angle formed by the vertical direction of the altitude and the incident vector \mathbf{n}' . At the altitude of 10 km, the intensity of the radiation coming from the lower atmosphere is >230 K, which is much stronger than that from the upper atmosphere (a few tens of Kelvin) at all the frequencies considered in this paper.

3.2 The microphysical model

In situ measurements have shown that cirrus clouds are composed of various non-spherical ice particles (McFarquhar and

Heymsfield, 1996). For our simulations we selected three types of ice particles to represent them: the nearly spherical particles, the circular cylinders, and the circular plates, for the ease of calculating the single scattering properties. All ice particles are assumed to be composed of pristine ice, which has a mass density of 0.92 g cm^{-3} . In describing ice particle size distributions, we used the maximum dimension to represent the particle size, which is the length for cylinders and the diameter for plates. For nearly spherical particles, the diameter of the mass equivalent sphere is used to define the particle size. In this paper, the maximum particle size is taken to be 2.0 mm and the minimum is $20 \mu\text{m}$. The size distribution is evaluated discretely for particle size from $20 \mu\text{m}$ to 2.0 mm with a fixed step of $20 \mu\text{m}$. This range of particle size is reasonable, because ice particles smaller than $20 \mu\text{m}$ are not significant enough for the mm and sub-mm wave scattering due to the very small volume fraction in clouds, although they may exist in a large number in realistic cirrus clouds (Lin et al., 1998). We assume the particle size distribution to be

$$N(D) = a D^\alpha e^{-\frac{\alpha+3.67}{D_m} D}, \quad (11)$$

where a is a normalization constant and α is the width parameter usually ranging from 0 to 2 (Evans et al., 1998). Parameter D_m is the median of the distribution of D to the third power, which separates the ice particles into two parts with equal mass, i.e. the total mass of ice particles with sizes smaller than D_m is equal to the total mass of ice particles with sizes larger than D_m . Since this distribution is discretely evaluated and also truncated at 2.0 mm of D , there will be a mass loss for the part with sizes larger than D_m . This mass loss will increase with D_m . Our calculations show that, for $\alpha = 1$, the mass loss is 1% of the total mass when D_m equals 0.8 mm. This loss increases to $\sim 4\%$ when D_m increases to 1.0 mm. The width parameter α was found to play a minor role in particle scattering properties, hence our following discussions will be limited to the case of $\alpha = 1$ (Lemke and Quante, 1999).

To calculate the single scattering parameters of ice particles, i.e. parameters $\tau_{s2,\beta}$ ($= N_0 \langle C_{sca,\beta} \rangle$) and $\langle Z_{21}(\mathbf{n}, \mathbf{n}') \rangle$, the T-Matrix method and the Discrete Dipole Approximation (DDA) method are used (Mishchenko and Travis, 1998; Draine and Flatau, 1998). $\langle C_{sca,\beta} \rangle$ is the ensemble-averaged scattering cross section of a single ice particle. Ensemble-averaging is done according to the given size, shape and orientation distributions. Because the T-Matrix method has a high computational efficiency, it is used in this study for most calculations of the single scattering properties. However, there are some cases when, perhaps because of the too large particle size and/or the aspect ratio, the T-Matrix code fails to converge. Then, the DDA method will be used to complement the T-Matrix method because it is more robust. The single scattering properties of the nearly spherical particles are calculated by averaging those from spheroid (both prolate and oblate), circular cylinders and circular plates, which

Table 1. The refractive index of pristine ice at a temperature of 250 K for the used mm and sub-mm frequencies

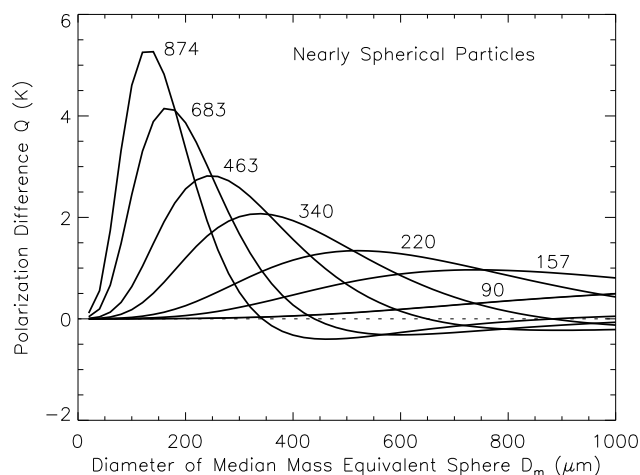
f(GHz)	λ (mm)	Real Part	Imaginary Part
90	3.333	1.7823	0.0026
157	1.910	1.7818	0.0039
220	1.364	1.7815	0.0049
340	0.882	1.7815	0.0067
463	0.648	1.7820	0.0084
683	0.439	1.7846	0.0111
874	0.343	1.7895	0.0134

have aspect ratios (η) of less than 1.5. The aspect ratio η denotes the ratio of the maximum to the minimum dimension of a non-spherical particle. In situ observations have shown that ice particle aspect ratios can change from 1 to 7 for cylinders and from 5 to 30 for plates (Auer and Veal, 1970). Following this information, our simulations are carried out for circular cylinders with η from 1 to 7 with a step of 1 and for circular plates with discrete η of 3, 5, 10, 20, and 30. The frequencies used are at 90, 157, 220, 340, 463, 683, and 874 GHz. Among these frequencies some (90, 157, 220, and 340 GHz) have been already tested in space-borne or air-borne sensors and some (463, 683, and 874 GHz) are recently found to be well matched in the atmospheric absorption comparisons and therefore they have been adopted by a new satellite mm/sub-mm radiometer concept (Miao et al., 2002). The refractive index of pristine ice at the used frequencies is given in Table 1, which is taken from the data set given by Warren (1984) and for a specific ambient temperature of 250 K.

3.3 The information content of the polarization signature

3.3.1 Cirrus clouds with randomly oriented ice particles

In this section, we consider ice clouds composed of randomly oriented ice particles. Although aerodynamic and gravitational forces tend to cause ice needles and plates, especially those with large size and aspect ratio, to have a preferred horizontal orientation for their longer axes (Brussaard and Watson, 1995), the orientation angle distribution for the whole ensemble of ice crystals varies from case to case (Chepfer et al., 1999). Therefore, random orientation is often a good approximation for ice particle orientations in cirrus clouds and it has been widely used in the retrievals of cirrus cloud parameters such as particle shape and IWP (Baran et al., 2001; Chepfer et al., 2001). For randomly oriented ice particles, $\tau_{s2,v}$ is equal to $\tau_{s2,h}$, which results in a vanishing second term on the righthand side of Eq. (9). Therefore, only the first term Q_s is needed to evaluate for the polarization sig-

**Fig. 2.** Simulated polarization differences for cirrus clouds composed of randomly oriented, nearly spherical ice particles. Results are shown for seven frequencies, which are in GHz and denoted above each curve. Detailed explanations are in the text.

nature. Q_s is zero for nadir-looking geometry and generally non-zero for non-nadir looking geometry. This is directly related to the symmetry or asymmetry distribution of the incident radiation intensity relative to the observation direction.

In Fig. 2 simulation results are shown for the case of nearly spherical particles. Please keep in mind that the satellite observation angle is 54° . The polarization difference Q is depicted against the ice particle characteristic size, which is represented by the diameter of the median mass equivalent sphere. Seven curves correspond to results at the seven frequencies which were mentioned in the preceeding section. The cirrus cloud is assumed to have an integrated ice water path of 60 gm^{-2} , which becomes 100 gm^{-2} along the slant satellite observation line with a zenith angle θ of 54° . Since only single scattering effect is considered in doing radiative transfer within the cloud, the simulation results given here can only be quantitatively used for thin clouds. Therefore, the values of the polarization difference Q given in Fig. 2 and in the following Figs. 3, 4, and 6 should be taken as the value per 60 gm^{-2} of cloud IWP, when the cloud IWP is other than 60 gm^{-2} .

It follows from Fig. 2 that, for a given frequency, Q is mainly sensitive to ice particles within a certain range of sizes. This feature is referred to as “resonance” in the following discussions. The magnitude of the resonance peak increases with increasing frequency (f). The peak position in particle size, denoted by D_m^* hereafter, also changes with frequency while the ratio of D_m^* and wavelength λ remains nearly constant (≈ 0.4). This feature tells us that high frequencies are more sensitive to smaller particles and lower frequencies are more sensitive to larger particles. Especially, when particle characteristic size D_m is less than $\sim 120 \mu\text{m}$, there exists a monotonic relationship between the polariza-

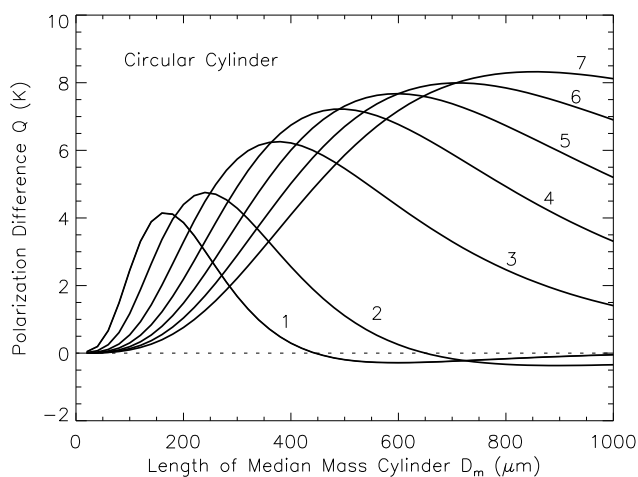


Fig. 3. Simulated polarization differences for cirrus clouds composed of randomly oriented circular cylinders with differing aspect ratios (denoted close to curves) at 683 GHz. Note, the particle characteristic size D_m represents the length of the median mass cylinder in this case.

tion difference Q and frequency f . Consequently, multi-frequency measurements of the polarization difference Q are potentially useful in determining ice particle characteristic size of cirrus clouds. However, this conclusion is limited to clouds with nearly spherical particles in random orientation.

If cirrus clouds are composed of other forms of particles, the results will be somewhat different. In Fig. 3 simulated polarization differences for circular cylinders are shown versus particle characteristic size. These results are for a fixed frequency of 683 GHz but with changing particle aspect ratios. Clearly, the aspect ratio of the ice particles plays a crucial role in the relations between the polarization difference Q and the particle characteristic size D_m . With the increase of particle aspect ratio, the magnitude of the resonance peak increases and the position of the peak moves toward large particles. When D_m is less than $\sim 150 \mu\text{m}$, Q is approximately inversely proportional to the aspect ratio, while D_m is larger than $\sim 700 \mu\text{m}$, Q becomes approximately directly proportional to the aspect ratio. Simulations for circular plates show similar results (see Fig. 4). However, difference is obvious for the two types of particles in the following two aspects. First, for plates the position of the resonance peak moves much more slowly with the increase of ice particle aspect ratio. Secondly, the magnitude of the resonance peak decreases slightly when the aspect ratio of plates changes from 20 to 30. This phenomenon does not appear for cylinders with aspect ratios less than 7. However, the two ranges of D_m , where a monotonic relationship exists for the polarization difference and the particle aspect ratio, are nearly identical for the two types of particles.

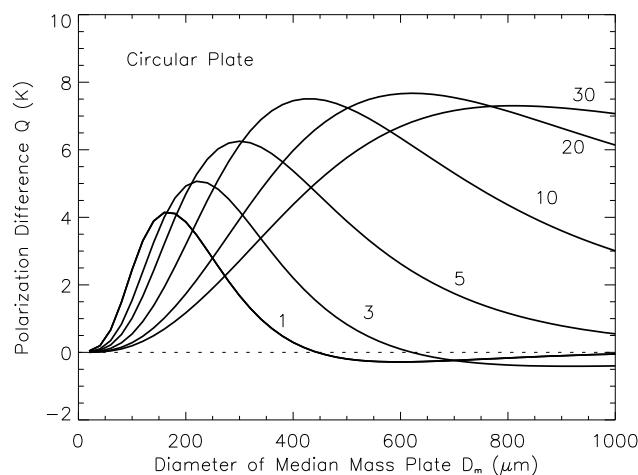


Fig. 4. Simulated polarization differences for cirrus clouds composed of randomly oriented circular plates with differing aspect ratios (denoted close to the curves) at 683 GHz. Note, the particle characteristic size D_m represents the diameter of the median mass plate in this case.

3.3.2 Effects of particle's orientations and shape mixtures

Natural ice clouds are a mixture of irregular ice particles with differing shapes and orientations. In this section we present two simple examples, in order to examine how these factors affect the polarization difference Q .

In examining particle orientation effect, we follow the procedure of Aydin and Tang (1997). Ice particles are assumed to be in simple forms, circular cylinder or circular plate, with the same aspect ratio. We assume that they have a preferred orientation angle relative to the horizontal plane but the particle axis is in a uniform distribution in the azimuth. The orientation angle δ is the angle formed by the axis of the largest dimension of the particle and the horizontal plane. For our simulations, orientation angle δ follows the truncated Gaussian function,

$$p(\delta) = \frac{1}{C_0} e^{-(\delta-\bar{\delta})^2/2\sigma_\delta^2}, \quad (12)$$

with the normalization constant C_0 expressed by

$$C_0 = \int_0^{\pi/2} e^{-(\delta-\bar{\delta})^2/2\sigma_\delta^2} \sin \delta d\delta. \quad (13)$$

The particle orientation angle δ changes in the range of $[0, \pi/2]$. The average orientation angle $\bar{\delta}$ is kept in zero in our simulations. This means, the ice particles lie in average on the horizontal plane. When the width parameter σ_δ changes from zero to infinity, ice particle orientation changes from one preferred direction gradually to randomness. Note, $\int_0^{\pi/2} p(\delta) \sin \delta d\delta = 1$.

Our simulations show that, when particles are oriented in a preferred direction, the polarization difference Q is gen-

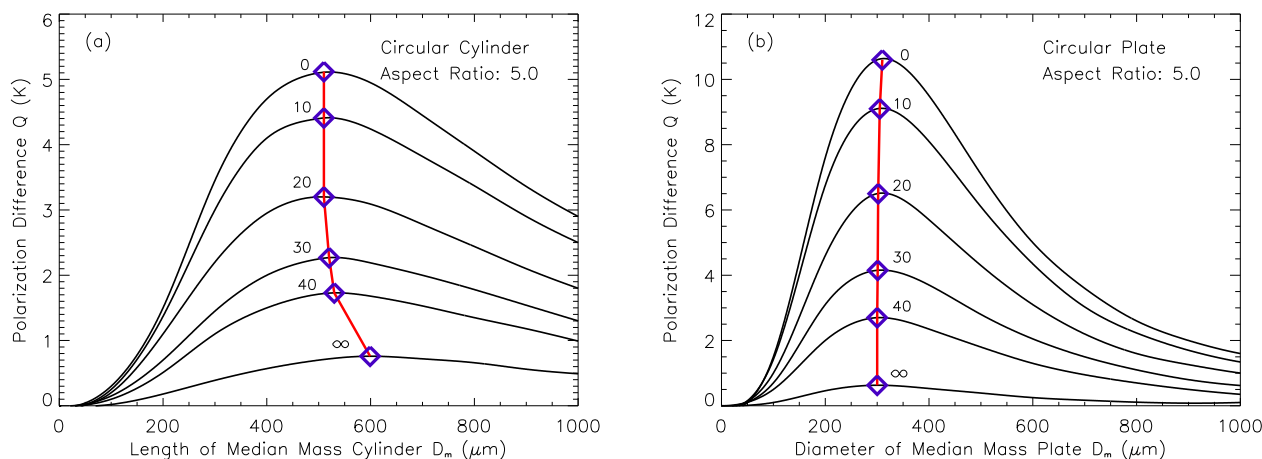


Fig. 5. Effect of particle orientation: The particle orientation angle δ follows a truncated Gaussian function described by Eqs. (12) and (13). The average orientation angle $\bar{\delta}$ is set to zero while the width parameter σ_δ changes from zero to infinity. $\sigma_\delta = 0$ means fully horizontal orientation and $\sigma_\delta = \infty$ means random orientation. The frequency is fixed at 683 GHz. Note, the value of Q shown here represents the polarization difference (in Kelvin) per 6 gm^{-2} of IWP. Diamond marks the position of the resonance peak.

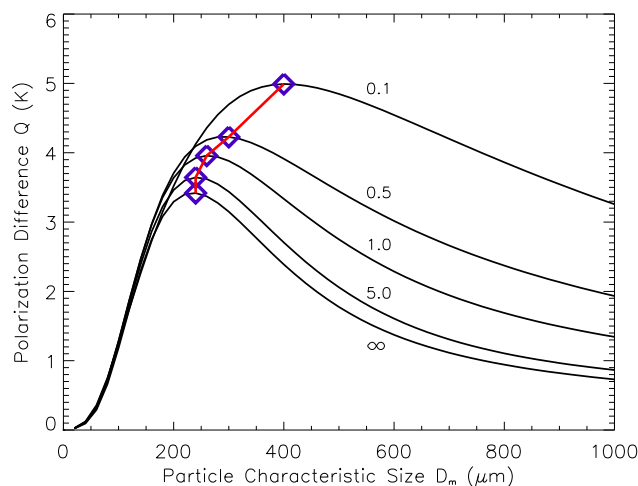


Fig. 6. Effect of particle shape mixture: Ice particles are a mixture of cylinders with differing aspect ratios from 1 to 7 and the number of each kind of cylinders is determined using a truncated Gaussian function (see details in text). The results shown correspond to width parameter σ_η changing from 0.1 to infinity. The frequency is fixed at 683 GHz. Note, Q should be taken as polarization difference (in Kelvin) per 60 gm^{-2} of ice water path. Diamond marks the position of the resonance peak.

erally larger than in the case of a random orientation. Especially, when σ_δ is zero, which means all particles are horizontally oriented, the value of Q at the resonance peak is several times larger than that in a random orientation: 8 times for circular cylinders and over 10 times for circular plates (see Fig. 5a and 5b). In general, orientation effect is more significant for plates than for cylinders. However, with the increase of width parameter σ_δ , Q decreases rapidly. When σ_δ equals 30° , Q at the resonance peak is already less than 50% of the value for the case of $\sigma_\delta = 0$. This is true for cylinders as well as for plates. It is noteworthy that the peak position D_m^* of Q in particle characteristic size changes little for plates when the orientation width parameter σ_δ changes

from zero to infinity. For cylinders, however, D_m^* initially remains nearly unchanged as σ_δ increases from zero to 20° . As σ_δ approaches infinity from 20° , D_m^* moves gradually from $\sim 500 \mu\text{m}$ to $\sim 600 \mu\text{m}$. Based on this simulation, we state that what we found for randomly oriented particles in the resonance feature of the polarization difference Q with respect to frequency, particle aspect ratio, and particle characteristic size, should remain to be similar for oriented particles. The only exception is that the magnitude of the resonance peak for oriented particles can be much larger than that of randomly oriented ice particles, depending on the width parameter σ_δ . We also noticed that particle orientation has a much more prominent effect than particle shape on the magnitude

of the resonance peak (compare Figs. 5a and 5b).

The effect of particle shape mixture is shown in Fig. 6, where the simulation results are given for circular cylinders. In this simulation, we assume ice particle numbers to be in a modified Gamma distribution in respect to particle size, as given in Eq. (11). However, ice particles at a certain size, denoted by the length of the circular cylinder, are composed of cylinders having equal lengths but with differing aspect ratios. The number fraction of ice particles in each aspect ratio is described by a discrete, truncated Gaussian function,

$$g(\eta) = \frac{1}{D_0} e^{-(\eta-\bar{\eta})^2/2\sigma_\eta^2}. \quad (14)$$

η denotes aspect ratio and takes discrete values from 1 to 7. D_0 is a normalization constant, enabling $\sum_{\eta=1}^7 g(\eta) = 1$. The average aspect ratio $\bar{\eta}$ increases linearly from 1 to 7 as the cylinder length increases from zero to 2.0 mm. The degree of shape mixture is controlled by the width parameter σ_η . Apparently, when σ_η is small, the particles at a certain length are composed mainly by cylinders with an aspect ratio corresponding to that length according to the linear relationship between $\bar{\eta}$ and particle length. When σ_η becomes larger and finally approaches infinity, particles will be composed of equal portions of cylinders with aspect ratios from 1 to 7.

The results in Fig. 6 show that shape mixture has influences on both the magnitude and the position of the resonance peak of the polarization difference Q . Compared with the results in Fig. 3, Q in Fig. 6 shows a considerably higher wing on the right hand side of the resonance peak, which extends to the large particle sizes. With an increasing width parameter σ_η , the behavior of polarization difference Q gradually becomes close to the case of cylinders with a small but fixed aspect ratio (compare Fig. 3). This is understandable. Since the volume of a cylinder with smaller aspect ratio is much larger than the volume of a cylinder of the same length but with a larger aspect ratio, particles with small aspect ratios will gradually dominate the volume of the ice particle ensemble, with the increase of the width parameter σ_δ . As a result, they will also gradually dominate the scattering effect.

Although shape mixture has a considerable influence on the polarization difference Q , the basic feature of Q in respect to the particle characteristic size does not change. This means, the polarization difference at a given frequency still shows its resonance for particles at a certain range of sizes, although the magnitude and position of the resonance peak may change depending on how the ice particles are mixed.

4 Conclusions

The main purpose of this study is to promote a general understanding of the potential of polarization measurements from space at mm/sub-mm wavelengths in determining cirrus clouds parameters but not to quantify the polarization signature of realistic cirrus clouds. To this end, simplified radiative transfer procedures have been pursued, which include

- (1) using single scattering to describe the interaction of the ice particles and atmospheric radiation;
- (2) ignoring the water vapor screening effect in the layers above the clouds; and
- (3) using circular cylinders, circular plates and nearly spherical particles to simulate natural ice particles.

Another important simplification included in our simulation is to omit the polarization signal from the ground surface, which may be significant for dry atmospheres especially at the millimeter wave frequencies.

Despite these simplifications introduced in the simulation, our results clearly show the unique features of polarization measurements. The most outstanding one is the resonance of the polarization difference for ice particles in a certain range of sizes. This resonance feature is also reported recently in a simulation and measurement study by Troitsky et al. (2001) for precipitating clouds at lower frequencies (≤ 85 GHz). Furthermore, we found that the position of the resonance peak in respect to particle size changes from large to small when the observing frequency increases from low to high. The position of resonance peak depends also on the particle shape and the aspect ratio. This resonance feature appears even when the particles are oriented or mixed with different shapes, although the exact magnitude and position of the resonance peak may change accordingly. This unique features of polarization difference with respect to particle microphysical properties suggest that polarization measurements from satellite at some well-chosen mm/sub-mm frequencies will benefit the determination of cirrus cloud parameters. In addition, polarization measurements in mm and sub-mm wavelengths are also an excellent complement to similar measurements in infrared and visible wavelength in determining microphysical properties of a wide range of cirrus clouds (Liou and Takano, 2002).

The results presented in the paper have been concentrated on a specific looking geometry of the satellite, i.e. the satellite zenith angle was fixed at 54° . In fact, we also examined the zenith angle dependence of the polarization difference Q , although the examination was limited to randomly oriented ice particles. We found that, for unit IWP along the observation direction, Q begins with a monotonic increase with the increase of the zenith angle. At about 60° to 70° of the zenith angle, Q reaches its maximum. Q goes down continuously from the maximum when the zenith angle approaches 90° . However, for a given cloud, the IWP along the observation path increases drastically with increasing zenith angle, therefore Q generally shows a monotonic increase trend when the satellite zenith angle varies from 0° to 90° .

Caution must be taken when trying to compare realistic measurements with the simulation results given in this study, especially when ice clouds are optically thick. Since multiple scattering has not been considered in the radiative transfer calculations, our simulation results are limited to optically

thin clouds. For example, at 683 GHz an ice cloud with an IWP of 6 gm^{-2} has an optical depth of less than 0.1, when the cloud is composed of circular ice cylinders with an aspect ratio of 5 and a median mass length of $500 \mu\text{m}$. If the single scattering radiative transfer can be taken to be valid for this case, then the polarization difference measured by a space-borne radiometer ranges from a few tenths of a Kelvin for randomly oriented particles to a few Kelvins for fully horizontally oriented particles (referring to Fig. 5a). As to the multiple scattering effect, our understanding is following. We should expect a linear increase of Q with the increase of cloud IWP in the range from zero to a certain amount, at which the multiple scattering effect begins to become significant. Beyond that amount of IWP, Q should gradually approach its saturation limit. In this process, the position of the resonance peak may change due to the variation of cloud optical depth with the change of ice particle size, even when the cloud IWP is fixed. The screening effect of the atmosphere in the layer on the top of the cloud is found to be negligibly small in the specific case which is discussed in this paper, since the transmittivity of this layer is high. At the highest frequencies (874 GHz) of our study it is larger than 0.95.

Future work will be focused on the quantitative determination of the polarization difference for various ice clouds composed of more realistic ice particles. Especially, the effects of multiple scattering effect and cloud inhomogeneity in both horizontal and vertical dimensions will be taken into account. For this purpose, a three-dimensional, fully-polarized radiative transfer model is under development in the Institute of Environmental Physics, University of Bremen (Kerridge et al., 2002). A cloud parameter retrieval scheme taking into account of the polarization measurements will also be developed.

Acknowledgements. This study was supported by the German AFO 2000 research program under grant 07ATC04 (Project UTH-MOS) and in part by the European Union under contract ENV4-CT98-0733.

References

- Auer, A. H. and Veal, D. L.: The dimensions of ice crystals in natural clouds, *J. Atmos. Sci.*, 27, 919–926, 1970.
- Aydin, K. and Tang, C.: Millimeter wave radar scattering from model ice crystal distribution, *IEEE Trans. Geosci. Remote Sensing*, 35, 140–146, 1997.
- Baran, A. J., Francis, P. N., Havemann, S., and Yang, P.: A study of the absorption and extinction properties of hexagonal ice columns and plates in random and preferred orientation, using exact T-matrix theory and aircraft observations of cirrus, *J. Quant. Spectrosc. Radiat. Transfer*, 70, 505–518, 2001.
- Brussaard G. and Watson, P. A: Atmospheric modelling and millimetre wave propagation, Chapman & Hall, London, UK, 1995.
- Chepfer, H., Brogniez, G., Goloub, P., Breon, F. M., and Flamant, P. H.: Observation of horizontally oriented ice crystals in cirrus clouds with POLDER-1/ADEOS-1, *J. Quant. Spectrosc. Radiat. Transfer*, 63, 521–543, 1999.
- Chepfer, H., Goloub, P., Riedi, J., DeHaan, J. F., Hovenier, J. W., and Flamant, P. H.: Ice crystal shapes in cirrus clouds derived from POLDER-1/ADEOS-1, *J. Geophys. Res.*, 106, 7955–7966, 2001.
- Draine, B. T. and Flatau, P.: User guide for the discrete dipole approximation code DDSCAT (Version 5a10), J Princeton Observatory Preprint POPE-xxx, 1998.
- Evans, K. F., Walter, S. J., Heymsfield, A. J., and Deeter, M. N.: Modeling of submillimeter passive remote sensing of cirrus clouds, *J. Atmos. Sci.*, 37, 184–205, 1998.
- Gasiewski, A. J.: Microwave radiative transfer in hydrometeors, *Atmospheric remote sensing by microwave radiometry*, (Ed) Janssen, M. A., John Wiley & Sons, Inc., pp. 91–144, 1993.
- Hollinger, J. P., Peirce, J. L., and Poe, G. A.: SSM/I instrument evaluation, *IEEE Trans. Geosci. Remote Sensing*, 28, 781–789, 1990.
- Kern, S. and Heygster, G.: Sea-ice concentration retrieval in the Antarctic based on the SSM/I 85.5 GHz polarization, *Annals of Glaciology*, 33, 109–114, 2001.
- Kerridge, B., Siddans, R., Latter, B., Dudhia, A., Lama, F., Stiller, G., v. Clarmann, T., Grabowski, U., Buehler, S., Miao, J., Emde, C., Murtagh, D., Eriksson, P., Lary, D., Mussa, H., Lee, A., and Baran, A.: Consideration of mission studying: Chemistry of the UTLS, Progress Report 2, ESTEC Contract No 15457/01/NL/MM, 2002.
- Lemke, H. M. and Quante, M.: Backscatter characteristics of non-spherical ice crystals: Assessing the potential of polarimetric radar measurement, *J. Geophys. Res.*, 104, 31 739–31 751, 1999.
- Lin, H., Noone, K. J., Ström, J., and Heymsfield, A. J.: Small ice crystals in cirrus clouds: A model study and comparison with in situ observations, *J. Atmos. Sci.*, 55, 1928–1939, 1998.
- Liou, K. N. and Takano, Y.: Interpretation of cirrus cloud polarization measurements from radiative transfer theory, *Geophys. Res. Lett.*, 29, 27,1–27,4, 2002.
- Liu, G. and Curry, J. A.: Determination of ice water path and mass median particle size using multichannel microwave measurements, *J. Appl. Meteor.*, 39, 1318–1329, 2000.
- Lynch, D. K., Sassen, K., Starr, D. O., and Stephens, G., *Cirrus*, Oxford University Press, Oxford, 2002.
- McFarquhar, G. M. and Heymsfield, A. J.: Microphysical characteristics of three anvils samples during the Central Equatorial Pacific Experiment, *J. Atmos. Sci.*, 53, 2401–2423, 1996.
- Miao, J., Johnsen, K.-P., Kern, S., Heygster, G., and Kunzi, K.: Signature of clouds over Antarctic sea ice detected by the Special Sensor Microwave/Imager, *IEEE Trans. Geosci. Remote Sensing*, 38, 2333–2344, 2000.
- Miao, J., Rose, T., Kunzi, K., and Zimmermann, P.: A future millimeter/sub-millimeter radiometer for satellite observation of ice clouds, *Int. J. Infrared and Millimeter Waves*, 23, 1159–1170, 2002.
- Mishchenko, M. I. and Travis, L.: Capabilities and limitations of a current fortran implementation of the T-Matrix method for randomly oriented, rotationally symmetric scatterers, *J. Quant. Spectrosc. Radiat. Transfer*, 60, 309–324, 1998.
- Mishchenko, M. I., Hovenier, J. W., and Travis, L. D.: *Light scattering by nonspherical particles: Theory, measurements, and application*, Academic Press, 2000.

- Spencer, R. W., Goodman, H. M., and Hood, R. E.: Precipitation retrieval over land with SSM/I: Identification of the scattering signal, *J. Atmos. Oceanic Technol.*, 6, 254–273, 1989.
- Troitsky, A. V., Osharin, A. M., Korolev, A. V., Strapp, W., and Isaa, G.: Studying the polarization characteristics of thermal microwave emission from a cloudy atmosphere, *Radiophysics and Quantum Electronics*, 44, 935–948, 2001.
- Ulaby, F. T., Moore, R. K., and Fung, A. K.: Microwave remote sensing: Active and passive, Artech House, Norwood, MA 02062, 1981.
- Wang, J. R., Liu, G., Spinhirne, J. D., Racette, P., and Hart, W. D.: Observation and retrievals of cirrus cloud parameters using multichannel millimeter-wave radiometric measurements, *J. Geophys. Res.*, 106, 15 251–15 263, 2001.
- Warren, S. G.: Optical constants of ice from the ultraviolet to the microwave, *Appl. Opt.*, 23, 1206–1223, 1984.